Research Article | Vol. 12, No. 5 / 1 May 2021 / Biomedical Optics Express 3008
Biomedical Optics EXPRESS

Raman spectroscopy for guidance of vulvar cancer surgery: a pilot study

HELENA C. VAN DOORN,[1,4] ELISA M. BARROSO,[2,4] SENADA KOLJENOVIĆ,[2] PATRICIA C. EWING-GRAHAM,[2] M. ROSA N. SOARES,[2] NICK J. VAN DE BERG,[1,*] TOM C. BAKKER SCHUT,[3] AND GERWIN J. PUPPELS[3]

[1]*Department of Gynaecologic Oncology, Erasmus MC Cancer Institute, Rotterdam, The Netherlands*
[2]*Department of Pathology, Erasmus MC, Erasmus University Medical Center, Rotterdam, The Netherlands*
[3]*Department of Dermatology, Erasmus MC, Erasmus University Medical Center, Rotterdam, The Netherlands*
[4]*shared first authorship*
[*]*n.vandeberg@erasmusmc.nl*

Abstract: For vulvar squamous cell carcinoma (VSCC), the mainstay of treatment is surgical removal with tumour-free margins. Surgeons still operate without objective tools that provide margin-status. This study assesses Raman spectroscopy potentiality for distinguishing ex-vivo VSCC from healthy tissue in 11 patients. Grid-based Raman maps were obtained from processed spectra. Water content and C-H band ratio (2,910-2,966 cm^{-1} / 2810-2890 cm^{-1}) were calculated per spectrum and used as linear discriminant parameters. Healthy tissue was differentiated from VSCC with 0.90 discriminative power, 0.79 sensitivity and 0.86 specificity.This is an important step towards the development of objective tools for VSCC surgical guidance.

1. Introduction

Vulvar cancer is a rare malignancy with an annual incidence in the Netherlands of 2.7/100,000 women [1]. However, the incidence has been increasing in recent years [1–4]. Eighty percent of all vulvar malignancies are vulvar squamous cell carcinoma (VSCC), and this tumour is associated with severe morbidity. The mainstay of treatment is surgical removal of the tumour with tumour-free margins. The European Society of Gynaecological Oncology (ESGO) recommends resection margins of at least 1cm [5]. However, there is no general agreement about the size of resection margin that is the most effective in reducing disease recurrence and disease-specific survival. Some studies have demonstrated that there is a higher risk of disease recurrence when the resection margins are less than 8 mm [6–8]. Yet other recent studies did not find any relation between the size of the resection margin and disease recurrence [9–15]. Moreover, it is known that other factors can contribute to local recurrence, such as multifocal tumour and the presence of dysplasia in the resection margins [8,16].

In practice, it is acceptable to consider less wide margins if the tumour is located close to midline structures, such as clitoris, urethra, sphincter ani and anus. Where margins are close, postoperative vulvar radiotherapy may be considered to reduce the risk of local recurrence. Again, there is no consensus on the minimal margin below which adjuvant radiotherapy is deemed necessary, although the Canadian guideline advises adjuvant radiotherapy where margins are < 8 mm [16].

While the size of margin required to significantly reduce the risk of recurrence remains a matter for debate, it is clear that positive-margins have a negative effect on patient outcome and must be avoided.

#420882 https://doi.org/10.1364/BOE.420882
Journal © 2021 Received 29 Jan 2021; revised 11 Mar 2021; accepted 29 Mar 2021; published 28 Apr 2021

Biomedical Optics EXPRESS

Histological evaluation by frozen section is the only method available for assessing margins during VSCC surgery. However, according to the Royal College of Obstetricians and Gynaecologists (2014), frozen sections are rarely used because they are not sufficiently representative of the final pathology (only a small portion of the wound bed or specimen is assessed). The outcome also depends on the experience of the surgeon and pathologist, and on the subjective assessment performed by both. Frozen section is also a time-consuming procedure [17,18].

As a result, surgeons still operate on VSCC patients without having any objective tool that can be used intraoperatively to assess the resection margins. In this pilot study we investigated whether such a tool might be realized with Raman spectroscopy.

Raman spectroscopy is an optical technique that provides detailed quantitative and qualitative information about the molecular composition of tissues. The technique is based on inelastic scattering of light by the molecules existing in tissue, is non-destructive and can be used directly on tissue without tissue preparation. Raman spectroscopy has proven to be a powerful candidate for in-vivo and ex-vivo intraoperative guidance of oncological surgical resections [19].

Our group has demonstrated the potential of this technique in differentiating squamous cell carcinoma of the oral cavity from the healthy surrounding tissue (both soft tissue and bone) and in determining the tumour border in soft tissue intraoperatively [19–21].

Although the use of Raman spectroscopy has been investigated for oral cavity SCC, Raman spectroscopy has not been used intraoperatively in VSCC. Therefore, the primary objective of this study is to assess ex-vivo the possibility of using Raman spectroscopy to distinguish VSCC from healthy surrounding tissue. This could be an important step towards the development of an objective tool to guide the surgeon in assessing the resection margin for VSCC, thus increasing the chance of oncologicaly radical surgery, reducing the need for post-operative treatment, and improving patient outcome.

2. Materials and methods

2.1. Medical ethical approval

This study was approved by the Medical Ethics Committee of Erasmus University Medical Center Rotterdam (MEC-2016-514). Informed consent was obtained from all included patients.

2.2. Tissue sampling and handling

Measurements were performed ex-vivo on resection specimens from patients undergoing surgery for VSCC. Immediately after resection, the surgeon pinned the specimen to cardboard and brought it to the pathology department, which was close to the operating room. The surgeon and the researcher documented the specimen with diagrams and digital images. The pathologist judged whether and what part of the specimen could be used for Raman spectroscopy measurements, without compromising normal pathologic assessment. After this, a cross-section (further called "Raman tissue section") with a thickness of about 5–10 mm was cut. The Raman tissue section was regarded as suitable when containing tumour and > 5 mm of surrounding normal-appearing tissue. Blood was rinsed from the Raman tissue section using physiological salt solution and the surface was gently patted dry with gauze. The Raman tissue section was inserted in a closed cartridge to avoid drying of the tissue. The upper side of the cartridge contains a fused silica window with a thickness of 1 mm, that allows scanning of a 3×3 cm^2 tissue area. The Raman tissue section was placed in the cartridge with the surface to be measured in contact with the fused silica window. Digital images of all handling steps were made, including images showing the macroscopic appearance of the tissue area measured.

After the experiment, the Raman tissue section was extracted from the cartridge. The experiments did not take longer than 60 minutes. Together with the rest of the specimen, the Raman tissue section was immersed in formalin (4%) to follow the routine procedure for final pathological processing. The whole experimental protocol is illustrated in Fig. 1.

Biomedical Optics EXPRESS

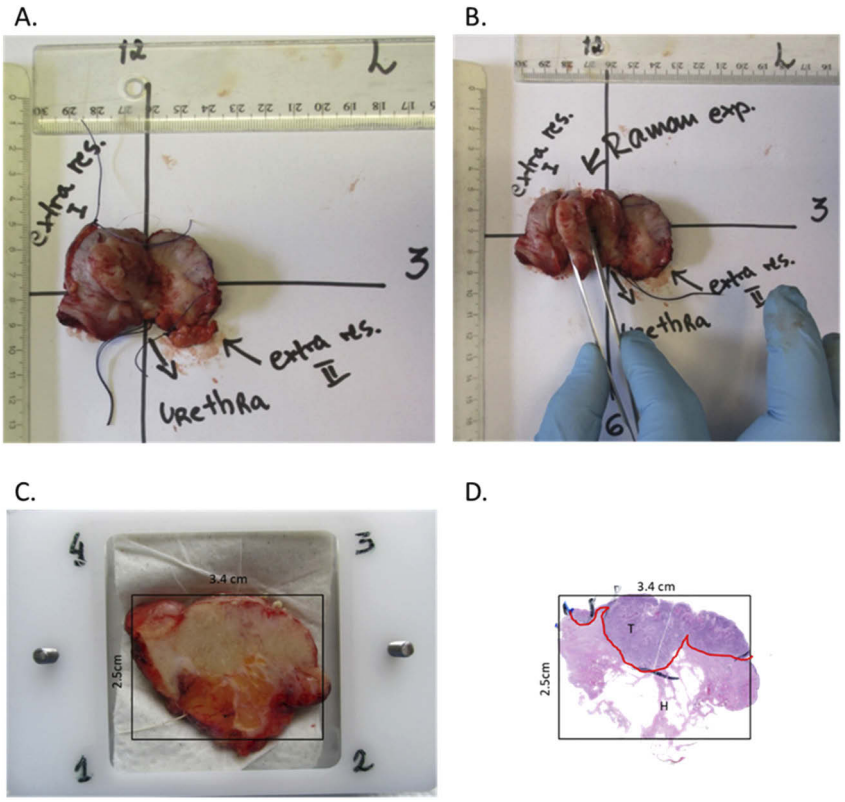

Fig. 1. Overview of the experimental protocol. A. Immediately after surgical resection, the specimen was brought by the surgeon to the pathology room, and the anatomical orientation in relation to midline structures was digitally recorded ('L' means left). B. Raman tissue section ('Raman exp.') was cut perpendicular to the resection surface. C. The Raman tissue section was inserted into a cartridge. The area to be measured, as defined by the surgeon and/or pathologist, containing tumour and surrounding healthy tissue. D. After performing Raman mapping experiments, the specimen was routinely processed, and a hematoxylin and eosin slide was made from the whole Raman tissue section measured. Histopathological annotation of tumour (T), healthy tissue (H), and of the tumour border (red line) was performed.

2.3. *Raman instrumentation and mapping experiments*

Raman ex-vivo mapping experiments were performed using a confocal Raman microscope (CRM) that was built in-house. The instrument was located in a laboratory close to the operating room and has been described in previous work [21]. For the measurements, 80 mW of laser light (wavelength: 671 nm) was focused on the tissue by means of a microscope objective. The objective magnification was 20x, the numerical aperture was 0.4, and the free working distance was 1.1 mm (N PLAN 11566026, Leica Microsystems BV). The depth resolution was 40 μm. Spectral information from the wavenumber range 2,500 to 4,000 cm^{-1} was obtained with a resolution < 5 cm^{-1}.

The cartridge with the tissue section was fastened on the microscope stage. The area of interest was measured point-by-point using a grid. The square grid cell size ranged between 350 and 1,000 μm, depending on the size of the Raman tissue section and taking into consideration that

Biomedical Optics EXPRESS

the sample should be measured in less than 60 minutes. The acquisition time per spectrum was 1 second. The laser light was focused at 50 μm in tissue below the fused silica window surface.

2.4. Calibration and pre-processing of spectra

All spectra were corrected for the wavelength-dependent detection efficiency of the setup and calibrated according to the instructions of the spectrometer supplier on the relative wavenumber axis (RiverD International BV, Rotterdam, The Netherlands). Cosmic ray events were removed, and the signal background generated in the optical path of the setup was subtracted [22]. MATLAB (Mathworks, Natick, MA, USA) was used for data processing and data visualization. Saturated spectra and spectra with a relative intensity lower than 5% of the average intensity of all spectra measured per Raman tissue section were discarded. The intensity of the spectra was determined for the range from 2,700 cm^{-1} to 3,100 cm^{-1}, containing spectral signatures from lipids and proteins. Low signal intensities were found at positions where the tissue was not in full contact with the measurement window. The method for determining and subtracting the fluorescence background signal in oral cavity tissues, using the multiple regression fitting method developed in [23], also functioned well in vulvar tissues.

2.5. Histopathologic annotation

Histopathologic evaluation of the measured areas was performed by two dedicated pathologists (PCE-G and SK) on routine hematoxylin and eosin (H&E)-stained thin tissue sections (5μm). The following information was assessed by the pathologists per Raman tissue section measured: main tissue structures present in the measured area, tumour differentiation grade, percentage of epithelium versus stroma in the tumour area, inflammation in or/and around the tumour, keratin in the tumour, necrosis in the tumour, and the presence of dysplasia (with the respective differentiation grade). Subsequently, the H&E-stained section was digitized, and the researcher and the pathologists delineated the tumour border in the digital image.

For each mapping experiment, the shape of the Raman tissue section measured was compared with the shape of the respective H&E-stained section. If there was a complete overlap between the shape of the Raman tissue section and the respective H&E-stained section, and if the measured area contained tumour, the mapping experiment was included for data analysis.

2.6. Data analysis

2.6.1. Spectral analysis

The analysis of spectra was performed in MATLAB. Spectral analysis consisted of four steps: 1) extraction of Raman features that have shown to be strong discriminators of SCC and healthy tissue in oral SCC [20,21]; 2) hierarchical cluster analysis (HCA) for identification of clusters that are located in tumour areas and clusters that are located in areas that contain healthy tissue; 3) analysis of spectral differences between these clusters, and 4) statistical analysis of the extracted features based on cluster results.

2.6.2. Extraction of Raman features

In previous studies, we have shown that the water content is significantly higher in SCC than in surrounding healthy tissue from the oral cavity [20,21]. We have also observed that the lipid to protein ratio based (ratio between C-H stretching bands located within the wavenumber region 2830 and 3020 cm^{-1}) of in tumour tissue was higher than in healthy bone [20].

Therefore, these two features were extracted from each spectrum, analyzed, and used to develop a VSCC classification model.

Biomedical Optics EXPRESS

Water percentage The water percentage was extracted by calculating the ratio of the signal intensity between the bands at 3390 cm^{-1} and 2935 cm^{-1} for each calibrated and background corrected spectrum according to the method developed and described in detail in previous studies [21,24,25].

C-H band ratio The C-H band ratio was calculated by dividing the area under the Raman signal in the spectral region 2,910 to 2,966 cm^{-1} by the area under the Raman signal in the spectral region 2810 to 2890 cm^{-1}. This calculation was performed for each calibrated and background corrected spectrum.

2.6.3. Hierarchical cluster analysis and histopathological annotation

A two-step HCA approach was chosen to limit the number of input spectra to the HCA as the time complexity is proportional to the square of the number of input events. In the first step, the spectra of a single map are clustered in a high number of clusters. Each cluster is represented by a cluster average. In the second step, the cluster averages of the full set of maps are clustered again to obtain a partition that associates the clusters with the histopathological annotation.

The wavenumber region between 2,800 and 3,050 cm-1 was used for a two-step HCA. This wavenumber region contains Raman signal that is mainly due to C-H stretching vibrations, which are highly present in biological samples. Before hierarchical cluster analysis, all spectra were scaled using an extended multiplicative scatter correction (EMSC) to eliminate the spectral interference of varying water contributions [25]. This method has been used in earlier studies and was used in this study to ensure that the analysis of the C-H stretching region is independent of the Raman signal obtained from water (OH-stretching).

Principal components analysis (PCA) was performed on the scaled spectra of each map to reduce the dimensionality of the data prior to hierarchical clustering. The scores of the first 20 PC's, accounting for more than 99.5% of the variance present in the data, were selected as input parameters of the hierarchical cluster analysis.

The first step of the hierarchical clustering consisted of a hierarchical cluster analysis per mapping experiment. Each map was clustered into 64 clusters using Ward's cluster algorithm and the Euclidean distance metric for pair wise distance measures. This number of clusters was chosen to ensure that all variance in the data set due to different tissue structures was well represented while limiting the number of input spectra to the second step. For each cluster, the average spectrum was calculated.

All cluster-averages from all maps were then used as input in the second step of the hierarchical cluster analysis, using the same algorithm and distance metric as in the first step. The results of the second step HCA were used to correlate the cluster membership with the histopathological annotation in the following way. A color code was associated with each second step HCA cluster and thereby all the first step HCA clusters that were part of that second step HCA cluster. For each Raman map, a cluster map was created by plotting the first step clustering as a 2D map using these associated cluster-colors.

The H&E-stained sections were manually projected onto the cluster maps, which allowed the correlation of each cluster with histopathology. This was done for different numbers of clusters to choose the optimal number of clusters in the second HCA step. In this optimum, each cluster could be clearly associated with one or more of the identified main tissue structures that can be encountered in vulvar specimens, and no cluster was associated with both healthy and tumour tissue. In this way, each cluster of the second HCA step, each cluster of the first HCA step, and, therefore, each single spectrum of each map was assigned to a single binary classifier: tumour or healthy tissue.

Biomedical Optics EXPRESS

2.6.4. Statistical analysis

For each extracted feature (water percentage and C-H band ratio), the mean, median, and standard deviation for the healthy tissue spectra group and tumour tissue spectra group were determined. A Mann-Whitney U-test was used to determine whether the distributions of the two groups were significantly different (CI: 95%) for each of the extracted features.

2.7. Development of a classification model for detection of VSCC

A linear discriminant analysis (LDA) model for the classification of VSCC was developed. The two extracted features (water percentage and C-H band ratio) of each single spectrum were used as input data for the model. As input classifier, a binary classifier, tumour or healthy, was used, as determined for each spectrum as described above.

The discriminative power of the LDA model was determined by calculating the area under the curve (AUC) of the receiver operating characteristic curve (ROC-curve) that was generated by evaluating the leave-one-patient-out prediction results for several discrimination threshold levels. The accuracy, sensitivity, and specificity of the multivariate linear discriminant model were determined at the discriminant threshold level determined by the Youden Index. The Youden Index is defined as the discriminant threshold level with the highest combined sensitivity and specificity [26].

3. Results

Twenty-one Raman mapping experiments were performed on fresh resection specimens from 21 patients who had VSCC surgery. Ten maps were excluded from the analysis because in four cases, there was not a complete overlap between the shape of the Raman tissue sections and the respective H&E-stained sections (an example is shown in Appendix A, Fig. 5(A), and in six cases, the measured area did not contain tumour (an example is shown in Appendix A, Fig. 5(B).

From the 11 included mapping experiments, a total of 8,281 spectra were measured. Each map had on average 753 spectra (range comprehended between 233 and 1,407 spectra) and an average area of 738 mm^2 (from 378 to 1,209 mm^2). Patient, tumour, and mapping experiment characteristics for the included data are shown in Table 1.

Table 1. Patient, tumour and mapping experiment characteristics. Patient number (N), patient's age, pathological TNM classification (pTNM), tumour differentiation grade, epithelial tumour vs stromal ratio, pixel size of the map performed (px), step size used during mapping experiments (mu), and number of spectra collected per patient (n).

Patient (N)	*Age*	*Diagnosis (VSCC)*	*Differentiation grade*	*(%)Epithelium/stroma within the VSCC*	*Map size (px)*	*Step size (mu)*	*Spectra (n)*
1	94	Recurrence	Moderate to well	70/30	36 × 23	1000	446
2	87	Recurrence	Moderate	60/40	35 × 26	1000	661
3	75	Recurrence	Well to poorly	70/30	39 × 31	1000	1032
4	53	Recurrence	Poorly	85/15	21 × 18	1000	233
5	90	T1b (palliative)	Poorly	25/75	57 × 19	350	1047
6	87	T1b (palliative)	Moderate	50/50	27 × 29	1000	587
7	64	Recurrence	Moderate to poorly	80/20	26 × 34	1000	700
8	83	T1N2M0, FIGO IIIC	Well	60/40	34 × 36	700	952
9	83	Recurrence	Moderate to poorly	70/30	39 × 25	500	693
10	89	T1b (palliative)	Moderate	75/25	36 × 37	700	1034
11	70	Recurrence	Well	85/15	25 × 38	500	896

Biomedical Optics EXPRESS

The main tissue structures observed in the H&E-stained slides of the measured Raman tissue sections were: tumour (VSCC), pre-existent epithelium (mucosa and skin), sebaceous glands, hair follicles, sweat glands, adipose tissue, muscle, blood vessels, nerves, fibrocollagenous tissue and fibromuscular stroma.

For each map, spectra were preprocessed and analyzed as described above. Twenty clusters resulted from the two steps HCA. Using a larger number of clusters in the second step of the HCA, we observed that clusters were formed based on their noise level and not based on actual differences in the Raman signal. Results obtained from the HCA are shown in Fig. 2. Macroscopic images of the measured areas, cluster maps, and annotated H&E-stained sections are shown for three patients (column A to C). The cluster averages that resulted from the HCA for all patients are shown in column D of Fig. 2. Clusters 14-17, 19, and 20 were identified as outliers due to low signal quality.

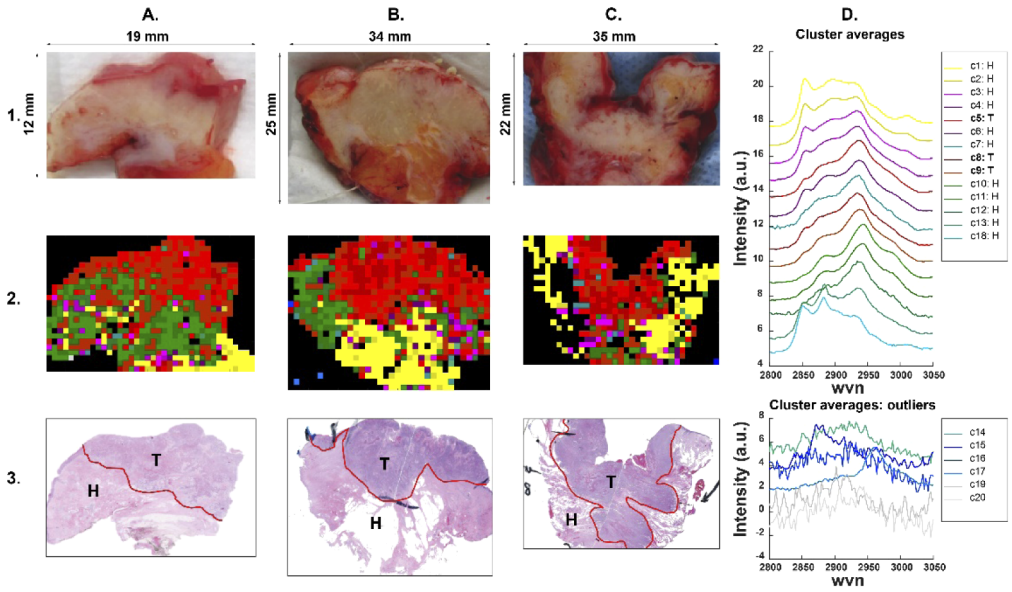

Fig. 2. Examples of HCA results for 3 Raman tissue sections from 3 patients (Column A-C). 1. Macroscopic photograph after insertion in the cartridge. 2. Cluster map color-coded according to the color of each cluster average (Column D). 3. Hematoxylin and eosin (H&E) stained section obtained from the measured Raman tissue section surface, with tumour border (red line), tumour (T), and healthy surrounding tissue (H) indicated by the pathologist. D. The 20 cluster averages (c1-c20) resulted from the hierarchical clustering analysis: 14 cluster averages were histopatholgically correlated to a specific tissue structure ('Cluster averages' graph) and 6 cluster averages were considered outliers ('Cluster averages: outliers' graph).

According to histopathological correlation, clusters 5, 8, and 9 were predominantly located in regions that contained tumour and mucosa (labelled as tumour), while the clusters 1-4, 6, 7, 10-13, and 18 were located around the tumour, where surrounding healthy tissue was present (labelled as healthy tissue). This is illustrated in Fig. 2. Regarding surrounding healthy tissue: clusters 1 and 2 were predominantly located in regions that contained adipose tissue; regions that mainly contained fibrocollagenous tissue and blood vessels coincided with the location of clusters 3, 4 and 6; big blood vessels corresponded to cluster 7; areas in Raman tissue sections that contained fibromuscular stroma corresponded to clusters 10, 11 and 12; and nerves corresponded to clusters 13 and 18.

Biomedical Optics EXPRESS

Figure 3 shows the results of the distribution analysis of the water percentage and C-H band ratio of the spectra labeled as tumour and the spectra labeled as healthy tissue. The mean water percentage in tumour was 79.15 ± 7.06. The mean C-H band ratio in tumour was 0.50 ± 0.05. The mean water content in healthy surrounding tissue was 54.41 ± 30.66%. The mean C-H band ratio in healthy tissue was 0.71 ± 0.31. For fibromuscular stroma the water content is 78.43 ± 4.90% and the C-H band ratio is 0.41 ± 0.05. For other healthy tissue types (without fibromuscular stroma) the mean water content is 34.70 ± 28.80% and the mean C-H band ratio is 0.96 ± 0.19. Tumour and healthy tissue water percentage distributions were significantly different ($p<0.01$). The bimodal distribution, shown in Fig. 3 A and B, in the C-H band ratio of healthy tissue is caused by fibromuscular stroma that has a C-H band ratio (0.41 ± 0.05) that is lower than that of tumour. Tumour and healthy tissue C-H band ratio distributions were significantly different ($p<0.01$).

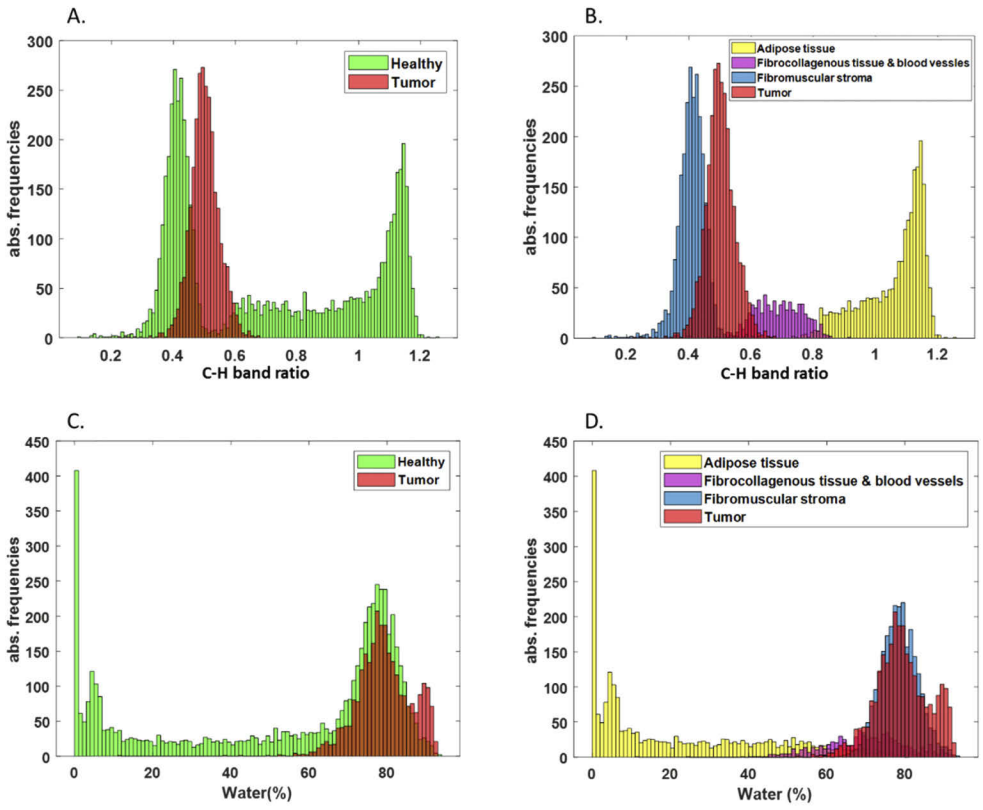

Fig. 3. Histograms of absolute frequencies for C-H band ratio (A and B) and water content (C and D) of healthy tissue spectra (adipose tissue, fibrocollagenous tissue, blood vessels, and fibromuscular stroma) and of tumour spectra.

An LDA model was created to classify spectra as 'healthy tissue' or 'tumour' using the water content and C-H band ratio as input parameters. The model was tested by leave-one-patient-out validation. Figure 4 shows the ROC curve of the validation test. The model has a high discriminative power (area under the curve) of 0.90, with a sensitivity of 0.79 and a specificity of 0.86 at the Youden index.

Biomedical Optics EXPRESS

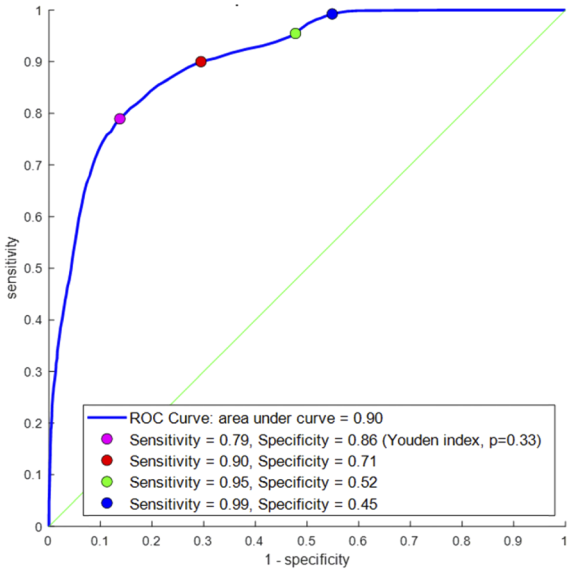

Fig. 4. ROC curve for leave one patient out validation of the LDA VSCC discrimination model based on water percentage and C-H band ratio.

4. Discussion

The aim of this pilot study was to assess the potential of Raman spectroscopy for guidance of vulvar SCC cancer surgery. Ex-vivo Raman mapping experiments were performed on freshly resected tissue to distinguish VSCC from healthy surrounding tissue.

VSCC and healthy vulvar tissue could be differentiated with a discriminative power of 90%, a sensitivity of 79% and a specificity of 86% using Raman spectroscopy. This was achieved by developing a linear discriminant model that was based only on two major discriminator parameters: the water content and the C-H band ratio. The water content (mean ± SD) in VSCC and healthy tissue (without fibromuscular stroma) was 79.15 ± 7.06% and 34.70 ± 28.80%, respectively. However, the water content of fibromuscular stroma (78.43 ± 4.90%) was similar to that of VSCC (79.15 ± 7.06%). The C-H band ratio of VSCC and fibromuscular stroma did differ and was 0.50 ± 0.05 and 0.41 ± 0.05, respectively. The mean C-H band ratio of healthy tissue (without fibromuscular stroma) was 0.96 ± 0.19.

To the authors' knowledge, this is the first study in which Raman spectroscopy is used to delineate VSCC and healthy vulvar tissue. In related applications, tissue was classified as vulvar lichen sclerosus or other inflammatory conditions (sensitivity 91%, specificity 80%) [27], and as healthy tissue or squamous cell carcinoma in the oral cavity region (sensitivity 99%, specificity 92%) [24]. A wider overview of Raman spectroscopy applications for cancer surgery guidance has been provided by Santos et al. [19].

How well Raman spectroscopy works for tissue classification hinges on the ability to identify distinctive tissue composition features through the spectra obtained. This can be done by using biologically descriptive features, such as water and lipid to protein content. Here, the C-H band ratio gives insight into the relative content of lipids and proteins in tissue [28]. These spectral features have been previously used to classify melanomas, [29] and tissue types in the cervix [30]. Alternatively, the PCA outcomes may be used as distinctive features for tissue classification. These principal components are abstract metrics missing a biological explanatory value. Nevertheless, they are independent factors that describe the data by definition, and they have already been matched with histopathology in the HCA step. It is, therefore, expected that their use will further improve LDA outcomes.

Biomedical Optics EXPRESS

Limitations of our study include the small cohort size in combination with the strict inclusion criteria drawn up to ensure a meaningful learning phase when matching histopathology with Raman spectra. In some specimens the Raman tissue section did not correlate to the H&E section most probably owing to tissue distortion during processing; the tissue could twist slightly in the course of processing perhaps in some cases as a result of the different tissue types present. Moreover, it is possible that pressure on the Raman tissue section by the cartridge during the measurements might explain why the tissue section and the form of the H&E section did not match in some cases. In addition, due to the different sizes of resected specimens, the step size of the grid-based analytical approach differed between 350 µm to 1000 µm. Finally, Raman acquisition and tissue handling in this training phase took up to 60 minutes. The time required will reduce when a trained optical probe is available. In the intended use, we expect to classify tissues in real-time.

Future work will include the exploration of additional distinctive features in the Raman spectra to refine our classification, e.g. to also enable the recognition of dysplastic tissues. In addition, the training phase will be extended to a larger cohort of patients, to better capture variation in spectra, within and between patients. Finally, the pilot required tissue handling and histopathological examination at the pathology department. Once a trained system is available, the technology may be used in the operating room to assess resected specimens directly. Alternatively, the technology may be expanded to scan the skin and mucosa in an outpatient clinic setting. This may provide insights about superficial spread of disease and assist in planning of treatments.

In conclusion, this study demonstrates that Raman spectroscopy can be used to discriminate VSCC from healthy vulvar tissue with a discriminative power of 90%. This study represents an important step towards the development of an objective tool for guiding resection of vulvar squamous cell carcinoma. Optimizing resection margins in this way could reduce the necessity for adjuvant treatment, and improve patient outcome.

Author's contributions

Conception and design: E.M. Barroso, H.C. van Doorn, T.C. Bakker Schut, P. Ewing-Graham, S. Koljenović, G.J. Puppels

Development of methodology: E.M. Barroso, T.C. Bakker Schut, S. Koljenović, G.J. Puppels

Acquisition of data (provided animals, acquired and managed patients, provided facilities, etc.): E.M. Barroso, H.C. van Doorn, P. Ewing-Graham, S. Koljenović.

Analysis and interpretation of data (e.g., statistical analysis, biostatistics, computational analysis): E.M. Barroso, T.C. Bakker Schut, P. Ewing-Graham, S. Koljenović, G.J. Puppels.

Writing, review, and/or revision of the manuscript: E.M. Barroso, H.C. van Doorn, T.C. Bakker Schut, N.J. van de Berg, M. Rosa N. Soares, P. Ewing-Graham, S. Koljenović, G.J. Puppels

Administrative, technical, or material support (i.e., reporting or organizing data, constructing databases): E.M. Barroso, H.C. van Doorn, S. Koljenović.

Study supervision: H.C. van Doorn, T.C. Bakker Schut, S. Koljenović, G.J. Puppels.

Biomedical Optics EXPRESS

Appendix A

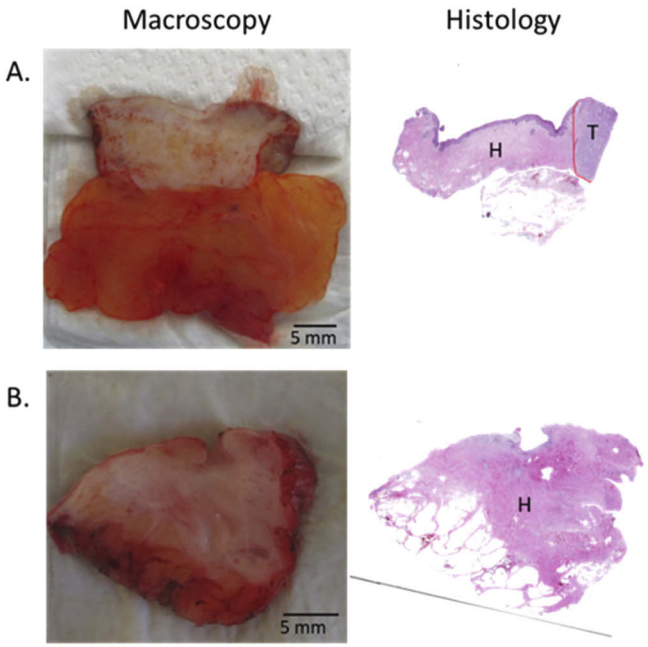

Fig. 5. Two examples (A and B) of Raman mapping experiments that were excluded. A. Macroscopic photograph after insertion in the cartridge with corresponding hematoxylin and eosin (H&E) slide. The histopathological annotation of tumour (T), healthy tissue (H), and of the tumour border (red line) is performed in the H&E slide. There is not a complete overlap between the shape of the Raman tissue section (Macroscopy) and the respective H&E-stained section (Histology). B. Macroscopic photograph after insertion in the cartridge with corresponding hematoxylin and eosin (H&E) slide. The histopathological annotation of healthy tissue (H) is performed in the H&E slide. The Raman tissue section does not contain tumour.

Disclosures. S. Koljenović, and G.J. Puppels have ownership interest (including patents) in RiverD International BV. T.C. Bakker Schut, M. Rosa N. Soares are employees of RiverD International BV. M. Rosa N. Soares is also employee of RiverD International BV. G.J. Puppels is employed with RiverD International BV as a CTO & Managing Director. No potential conflicts of interest were disclosed by the other authors.

References

1. M. S. Schuurman, L. C. van den Einden, L. F. Massuger, L. A. Kiemeney, M. A. van der Aa, and J. A. de Hullu, "Trends in incidence and survival of Dutch women with vulvar squamous cell carcinoma," Eur. J. Cancer **49**(18), 3872–3880 (2013).
2. F. Bray, M. Laversanne, E. Weiderpass, and M. Arbyn, "Geographic and temporal variations in the incidence of vulvar and vaginal cancers," Int. J. Cancer **147**(10), 2764–2771 (2020).
3. S. Mancini, L. Bucchi, F. Baldacchini, O. Giuliani, A. Ravaioli, R. Vattiato, M. Preti, R. Tumino, S. Ferretti, A. Biggeri, A. Brustolin, L. Boschetti, A. L. Caiazzo, A. Caldarella, R. Cesaraccio, C. Cirilli, A. Citarella, R. A. Filiberti, M. Fusco, R. Galasso, L. Gatti, F. L. Lotti, M. Magoni, L. Mangone, G. Masanotti, G. Mazzoleni, W. Mazzucco, A. Melcarne, M. Michiara, P. Pesce, S. Piffer, A. Pinto, M. Rognoni, S. Rosso, M. Rugge, G. Sampietro, S. Scalzi, T. Scuderi, G. Tagliabue, F. Tisano, F. Toffolutti, S. Vitarelli, F. Falcini, and A. W. Grp, "Incidence trends of vulvar squamous cell carcinoma in Italy from 1990 to 2015," Gynecol. Oncol. **157**(3), 656–663 (2020).
4. C. L. Rasmussen, L. T. Thomsen, G. L. Aalborg, and S. K. Kjaer, "Incidence of vulvar high-grade precancerous lesions and cancer in Denmark before and after introduction of HPV vaccination," Gynecol. Oncol. **157**(3), 664–670 (2020).
5. ESG Oncology, "Vulvar Cancer Guidelines," 1–75 (2017).
6. E. L. Barlow, M. Jackson, and N. F. Hacker, "The prognostic role of the surgical margins in squamous vulvar cancer: a retrospective Australian study," Cancers **12**(11), 3375 (2020).

Biomedical Optics EXPRESS

7. J. K. Chan, V. Sugiyama, H. Pham, M. Gu, J. Rutgers, K. Osann, M. K. Cheung, M. L. Berman, and P. J. DiSaia, "Margin distance and other clinico-pathologic prognostic factors in vulvar carcinoma: A multivariate analysis," Gynecol. Oncol. **104**(3), 636–641 (2007).
8. G. Baiocchi, H. Mantoan, L. de Brot, L. Badighan, L. Y. Kumagai, C. C. Faloppa, and A. A. B. A. da Costa, "How important is the pathological margin distance in vulvar cancer?" Eur. J. Surg. Oncol. **41**(12), 1653–1658 (2015).
9. S. M. A. Groenen, P. J. Timmers, and C. W. Burger, "Recurrence rate in vulvar carcinoma in relation to pathological margin distance," Int. J. Gynecol. Cancer **20**(5), 869–873 (2010).
10. L. S. Nooij, F. A. M. Brand, K. N. Gaarenstroom, C. L. Creutzberg, J. A. de Hullu, and M. I. E. van Poelgeest, "Risk factors and treatment for recurrent vulvar squamous cell carcinoma," Crit. Rev. Oncol. Hematol. **106**, 1–13 (2016).
11. N. Pleunis, M. E. J. Leermakers, A. A. van der Wurff, P. J. J. M. Klinkhamer, N. P. M. Ezendam, D. Boll, J. A. de Hullu, and J. M. A. Pijnenborg, "Surgical margins in squamous cell carcinoma, different for the vulva?" Eur. J. Surg. Oncol. **44**(10), 1555–1561 (2018).
12. N. C. te Grootenhuis, A. W. Pouwer, G. H. de Bock, H. Hollema, J. Bulten, A. G. J. van der Zee, J. A. de Hullu, and M. H. M. Oonk, "Margin status revisited in vulvar squamous cell carcinoma," Gynecol. Oncol. **154**(2), 266–275 (2019).
13. L. Woelber, L. F. Griebel, C. Eulenburg, J. Sehouli, J. Jueckstock, F. Hilpert, N. de Gregorio, A. Hasenburg, A. Ignatov, P. Hillemanns, S. Fuerst, H. G. Strauss, K. H. Baumann, F. C. Thiel, A. Mustea, W. Meier, P. Harter, P. Wimberger, L. C. Hanker, B. Schmalfeldt, U. Canzler, T. Fehm, A. Luyten, M. Hellriegel, J. Kosse, C. Heiss, P. Hantschmann, P. Mallmann, B. Tanner, J. Pfisterer, B. Richter, P. Neuser, and S. Mahner, "Role of tumour-free margin distance for loco-regional control in vulvar cancer-a subset analysis of the Arbeitsgemeinschaft Gynakologische Onkologie CaRE-1 multicenter study," Eur. J. Cancer **69**, 180–188 (2016).
14. L. Woelber, M. Choschzick, C. Eulenburg, M. Hager, F. Jaenicke, F. Gieseking, L. Kock, M. Ihnen, C. Petersen, J. Schwarz, and S. Mahner, "Prognostic value of pathological resection margin distance in squamous cell cancer of the vulva," Ann. Surg. Oncol. **18**(13), 3811–3818 (2011).
15. J. M. Heaps, Y. S. Fu, F. J. Montz, N. F. Hacker, and J. S. Berek, "Surgical-pathologic variables predictive of local recurrence in squamous cell carcinoma of the vulva," Gynecol. Oncol. **38**(3), 309–314 (1990).
16. J. A. Francis, L. Eiriksson, E. Dean, A. Sebastianelli, B. Bahoric, and S. Salvador, "No. 370-management of squamous cell cancer of the vulva," J. Obstet. Gynaecol. Can. **41**(1), 89–101 (2019).
17. L. C. Horn and S. Wagner, "Frozen section analysis of vulvectomy specimens: results of a 5-year study period," Int. J. Gynecol. Pathol. **29**(2), 165–172 (2010).
18. T. Crowley, "Guidelines for the diagnosis and management of vulval carcinoma," *Royal College of Obstetricians and Gynaecologists*, 1–35 (2014).
19. I. P. Santos, E. M. Barroso, T. C. B. Schut, P. J. Caspers, C. G. F. van Lanschot, D. H. Choi, M. F. van der Kamp, R. W. H. Smits, R. van Doorn, R. M. Verdijk, V. N. Hegt, J. H. von der Thusen, C. H. M. van Deurzen, L. B. Koppert, G. J. L. H. van Leenders, P. C. Ewing-Graham, H. C. van Doorn, C. M. F. Dirven, M. B. Busstra, J. Hardillo, A. Sewnaik, I. ten Hove, H. Mast, D. A. Monserez, C. Meeuwis, T. Nijsten, E. B. Wolvius, R. J. B. de Jong, G. J. Puppels, and S. Koljenovic, "Raman spectroscopy for cancer detection and cancer surgery guidance: translation to the clinics," Analyst **142**(17), 3025–3047 (2017).
20. E. M. Barroso, I. ten Hove, T. C. B. Schut, H. Mast, C. G. F. van Lanschot, R. W. H. Smits, P. J. Caspers, R. Verdijk, V. N. Hegt, R. J. B. de Jong, E. B. Wolvius, G. J. Puppels, and S. Koljenovic, "Raman spectroscopy for assessment of bone resection margins in mandibulectomy for oral cavity squamous cell carcinoma," Eur. J. Cancer **92**, 77–87 (2018).
21. E. M. Barroso, R. W. H. Smits, C. G. F. van Lanschot, P. J. Caspers, I. ten Hove, H. Mast, A. Sewnaik, J. A. Hardillo, C. A. Meeuwis, R. Verdijk, V. N. Hegt, R. J. B. de Jong, E. B. Wolvius, T. C. B. Schut, S. Koljenovic, and G. J. Puppels, "Water concentration analysis by Raman spectroscopy to determine the location of the tumor border in oral cancer surgery," Cancer Res. **76**(20), 5945–5953 (2016).
22. R. Wolthuis, T. C. Bakker-Schut, P. J. Caspers, H. P. J. Buschman, T. J. Römer, H. A. Bruining, and G. J. Puppels, "Raman spectroscopic methods for in vitro and in vivo tissue characterization," in *Fluorescent and Luminescent Probes for Biological Activity* (Elsevier, 1999), pp. 433–455.
23. E. M. Barroso, T. C. B. Schut, P. J. Caspers, I. P. Santos, E. B. Wolvius, S. Koljenovic, and G. J. Puppels, "Characterization and subtraction of luminescence background signals in high-wavenumber Raman spectra of human tissue," J. Raman Spectrosc. **49**(4), 699–709 (2018).
24. E. M. Barroso, R. W. H. Smits, T. C. B. Schut, I. ten Hove, J. A. Hardillo, E. B. Wolvius, R. J. B. de Jong, S. Koljenovic, and G. J. Puppels, "Discrimination between Oral cancer and healthy tissue based on water content determined by Raman spectroscopy," Anal. Chem. **87**(4), 2419–2426 (2015).
25. H. Martens and E. Stark, "Extended multiplicative signal correction and spectral interference subtraction - new preprocessing methods for near-infrared spectroscopy," J. Pharm. Biomed. Anal. **9**(8), 625–635 (1991).
26. W. J. Youden, "Index for rating diagnostic tests," Cancer **3**(1), 32–35 (1950).
27. J. Frost, L. Ludeman, K. Hillaby, R. Gornall, G. Lloyd, C. Kendall, A. C. Shore, and N. Stone, "Raman spectroscopy and multivariate analysis for the non invasive diagnosis of clinically inconclusive vulval lichen sclerosus," Analyst **142**(8), 1200–1206 (2017).
28. A. C. S. Talari, Z. Movasaghi, S. Rehman, and I. U. Rehman, "Raman spectroscopy of biological tissues," Appl. Spectrosc. Rev. **50**(1), 46–111 (2015).

Biomedical Optics EXPRESS

29. I. P. Santos, P. J. Caspers, T. C. B. Schut, R. van Doorn, V. N. Hegt, S. Koljenovic, and G. J. Puppels, "Raman spectroscopic characterization of melanoma and benign melanocytic lesions suspected of melanoma using high-wavenumber Raman spectroscopy," Anal. Chem. **88**(15), 7683–7688 (2016).
30. J. H. Mo, W. Zheng, J. J. H. Low, J. Ng, A. Ilancheran, and Z. W. Huang, "High Wavenumber Raman Spectroscopy for in Vivo Detection of Cervical Dysplasia," Anal. Chem. **81**(21), 8908–8915 (2009).